A Revolutionary Approach to Individual Electric Scooter, Design and Implementation

Markel Etxabe, Ioritz Iribar, Jon Ander Juaristi, Ander Merino, Axier Zeberio

***Abstract*— To promote electric mobility, an electric scooter has been designed and built. This scooter is specifically crafted to have enough autonomy to cover the route from the center of Donosti to Bidebieta, 3.2 km, with a consumption rate of 16.5 Wh. The electrical and mechanical systems have been analyzed to effectively control the scooter's speed, utilizing a PI controller. In addition, our lithium-ion battery has been modeled to operate within the range of 20V to 29.4V, simulating the consumption the battery will experience. The analysis indicates a moderate discharge, reaching up to 84% state of charge (SoC). For recharging the battery, a charging station has been designed, obtaining energy from a single PV panel. This charging station is capable of simultaneously charging 20 scooters, powered by a Lithium LiFePO4 24V 100Ah battery, ensuring a stable energy supply. The charging station is equipped with air conditioning to maintain a consistent temperature of 20ºC and a relative humidity of 50%.**

***Index Terms*— Electric mobility, Scooter, Daily route, DC chopper, Efficiency, Controller, PV panel, Charging station, Hydrogen.**

I. Introduction

Electric mobility has become one of the most relevant trend in the automotive sector in the last decade. However, in Spain there is a strong habit towards gasoline-powered vehicles. Therefore, the Spanish government has decided to act by implementing the law of climate change and energy transition act [1]. The aim of this law is to catch up the Paris Agreement, settled by the EU. In Spain, the automotive sector is the responsible of the %27 of CO_2 emissions [2]. Furthermore, %86 of CO_2 urban emissions are due to mobility [3]. Meaning citizens tend to make use of the car for distances within the city.

The solution the government suggests is to increase the use of public transport and electric mobility. Concerning electric vehicles %12 of vehicle registrations was from hybrid and electric vehicles. Those are poor numbers compared to the Eurozone, which count with %30 [4] . The main drawback electric mobility presents is its cost. The current market does not count with cheap alternatives. Regular people tend to look closely at the price when buying a vehicle. As a solution, some enterprises like *Sanitas* provide employees with bus services, electric scooters and free electric bicycles. Thanks to this alternative *Sanitas* has avoided the emission of more than 120 tonnes of CO_2 [5].

A. Sustainable Development Goals

Given that less than 40% of global urban areas are serviced by public transportation, scooters offer a viable means to enhance individual mobility. Consequently, there is a direct and positive impact on objectives 11-2, 11-3, and 11-6, aligning with the development of sustainable cities and communities.

A positive correlation exists with objective 3-9, which focuses on the health and wellbeing of the population. This correlation is particularly advantageous for individuals living in densely populated areas.

The battery charging processes are intentionally structured to take place at charging stations utilizing photovoltaic panels. This approach encourages the adoption of renewable generation technologies, thereby contributing to the expansion of universal access to modern energy sources, increasing the overall capacity of installed renewable power, and enhancing energy efficiency. Additionally, ongoing research into harnessing hydrogen as an energy source for the scooter further supports the advancement of clean and accessible energy. These initiatives align with objectives 7-1, 7-2, 7-3, and 7-A, which focus on sustainable energy development.

On the other hand, not all impacts are positive. Our scooter, with its lithium-ion batteries, could potentially have adverse effects on ecosystems if not properly managed after degradation. This directly relates to goal 15-1.

II. Prototype description

It has been developed an innovative electric scooter with a primary focus on the energy supply system. The project involved harnessing solar energy through strategically positioned solar panels, which were integrated into a specialized charging station equipped with cooling and humidity control systems maintained by air conditioning technology.

Within this advanced charging station, a high-performance lithium-ion battery was efficiently recharged, ensuring optimal energy storage for the electric scooter. The stored energy was directed to power a precision-crafted DC motor, with initial processing through a dedicated DC converter.

The DC converter in the system was intricately managed by a Texas microcontroller. This microcontroller dynamically adjusted the Pulse Width Modulation (PWM) signal, aligning it with the precise voltage and current requirements of the electric scooter. This meticulous control mechanism ensured an efficient and tailored energy delivery, optimizing the

scooter's performance while enhancing overall energy utilization.

These advancements represent a significant step forward in the development of sustainable and efficient electric mobility solutions. The integration of solar energy harvesting, advanced battery technology, and precision control systems contributes to the overall optimization of energy consumption in electric scooters, as detailed in this scientific paper.

Additionally, the possibility of incorporating hydrogen fuel cells soon was explored as an intriguing and revolutionary topic in the energy field.

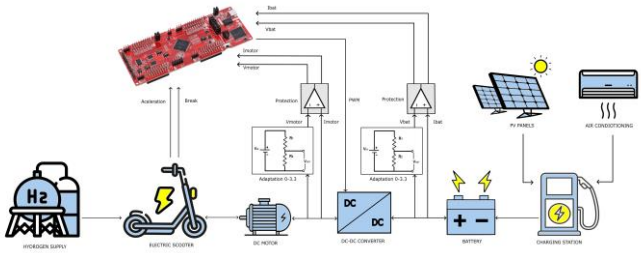

Figure 1 The representation of the entire system

A. *Objectives*

Once the decision was made to focus on a specific type of product or vehicle, namely the electric scooter, a set of objectives and requirements were established for the project. The aim was to address the issues mentioned in (I) and cater to the maximum needs and desires of potential consumers of the vehicle. The primary goal of this project is to create and implement a lightweight electric scooter within a three-month timeframe, providing a flexible solution for individual transportation within the city.

To achieve this overarching goal, the following sub-objectives were outlined.

- Achieve a range of 4 km on level ground.
- Design a PV panels-based charging station for 20 scooters.
- Keep the charging station around 20 degrees and a relative humidity of below 50%.
- Achieve an efficiency of at less 97% in the DC-DC converter.
- Develop a design with a maximum weight of 15 kg to ensure lightness.

III. SYSTEM ENERGETIC ANALYSIS

A. *Specifications*

To analyze the system energetically, many specifications were decided. Shown in the TABLE I, these specifications correspond to the engine, electronic components, and certain assumptions. To obtain the desired results, selecting limitations is a must.

TABLE I
ENERGETIC LIMITATIONS

Passenger mass	80kg
Scooter mass	30 kg
Current max/min	±27 A
Coefficient of friction	0.004 [11]
Minimum route	3 km
Gravitational acceleration	9.81 m/s^2
Wheel radius	0.15 m

B. *Design*

First, the route of the electric scooter was selected as shown in *Figure 2*. The picture was obtained from Google Maps and then converted to a GPX file.

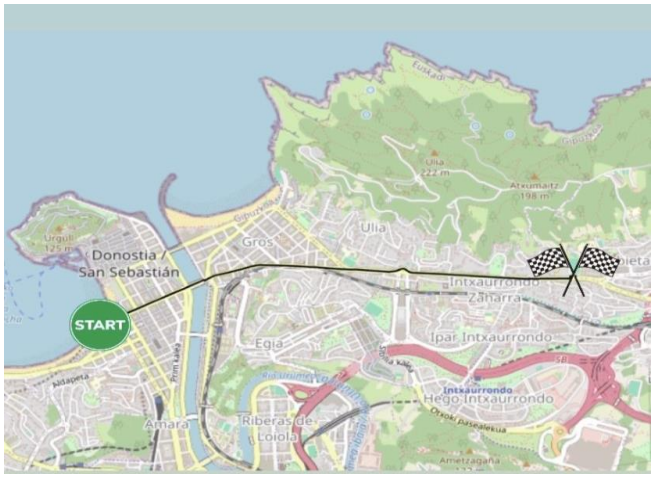

Figure 2 The route is selected to be in Donostia, going from the city center to a football field in Bidebieta. Its total distance is 3.2km and it was chosen due to is simplicity.

Furthermore, the latitude, longitude, and elevation data were acquired. Utilizing this information, the intervals between coordinate points for both latitude and longitude were computed using the haversine function. The distances between each point and the corresponding angles were also calculated, being the outcomes presented in *Figure 3*.

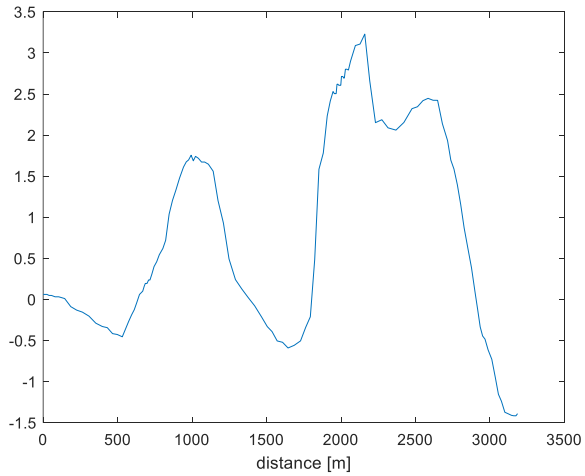

Figure 3 The elevation the scooter will face during the route. As the profile changed dramatically in few meters the data was smoothed, using a Smooth Data function in MATLAB.

In order to know how the scooter will act to the elevation of the route, a speed profile was created. Being 25 km/h the maximum speed permitted for an electric scooter by the DGT [6], different speed values were assigned to the angle values. As the slope of the profile increases, the scooter needs a higher power to maintain its speed; so, higher speed values have been assigned to smaller slopes, obtaining *Figure 4*.

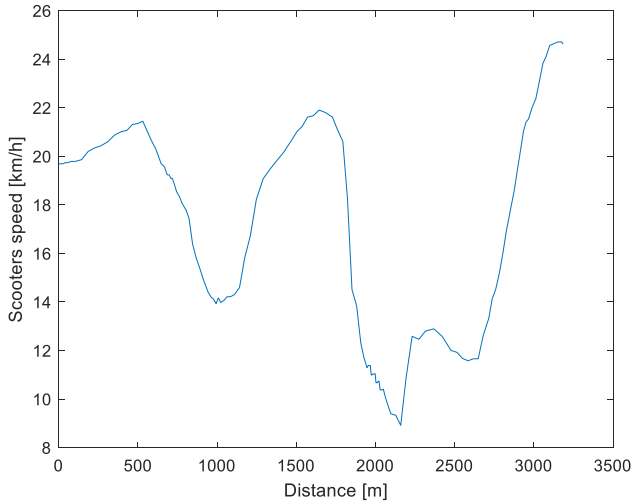

Figure 4 The speeds profile during the route with the selected speed requirements, minimum 6 km/h and maximum 25 km/h [6].

Moreover, scooters' force diagram was done to obtain the mechanical power and energy the scooter would consume.

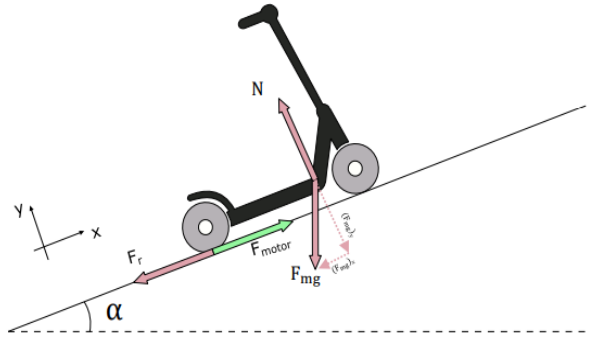

Figure 5 Mechanical model of the electric scooter.

Assuming power on the wheel will be the same as power on the motor, the mechanical response of the system was analyzed by the following equations (1, (2. Shown in Figure 6.

$$W_{motor} = \left(F_r + F_{(mg)x}\right) dx \qquad (1)$$

$$P_{motor} = \frac{W_{motor}}{dt} \qquad (2)$$

The variable *dx* was extracted from the route as it is its distance variation. However, *dt* was calculated with equation (3.

$$dt = \frac{dx}{v_{scooter}} \qquad (3)$$

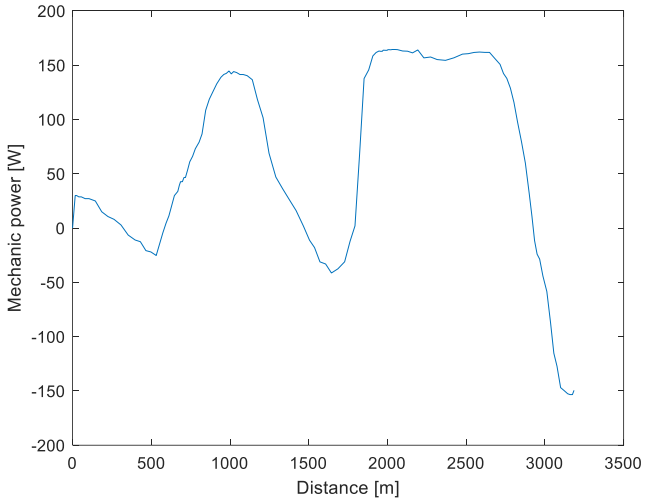

Figure 6 Mechanical power in the motor during the route. Considering mechanical power in the wheels would be the same as in the motor.

Additionally, using the relation of gears between the DC motor and the pinon, the angular speed of the motor was calculated (4)*(5)*. For this, it was necessary to assume that the pinon and the motor are connected through an ideal chain.

$$\omega_{\text{motor}} = \frac{\omega_{\text{wheel}}}{n} \quad (4)$$

$$n = \frac{z_{wheel}}{z_{\text{motor}}} \quad (5)$$

By analyzing these variables and considering the assumed ideal chain connection, it became possible to compute the mechanical torque exerted by the motor.

$$T_{\text{motor}} = \frac{P_{\text{motor}}}{\omega_{\text{motor}}} \quad (6)$$

Finally, after obtaining all these variables, they were assembled in a graphic, Figure 7.

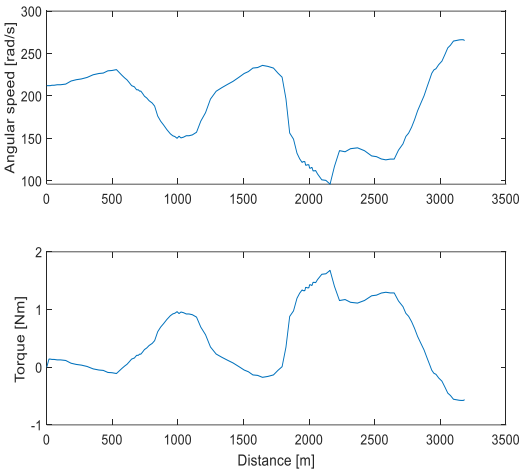

Figure 7 Angular speed and torque in the motor.

Certainly, the angular velocity exhibits a closely resembling pattern to linear velocity, given their connection through a constant, the radius of the wheel. Conversely, power and torque exhibit an inverse relationship: as speed increases (and the angle decreases), less power and consequently less torque are required. However, when speed decreases, the power and torque necessary for traversing that incline are heightened. Additionally, in negative angles (downhill), the scooter moves under the influence of gravity, leading to regeneration and battery charging, resulting in negative values for power and torque. Subsequently, with the motor torque determined, the motor current has been calculated using equation (*7*) . Being the motor voltage constant obtained from the TABLE.

$$i_a = \frac{T_{\text{motor}}}{k_{\text{e}}} \quad (7)$$

Firstly, when the motor current profile was obtained the system was not able to provide it, considering its maximums and minimums. Therefore, the route was modified with the aim of fixing the current profile, Figure 8.

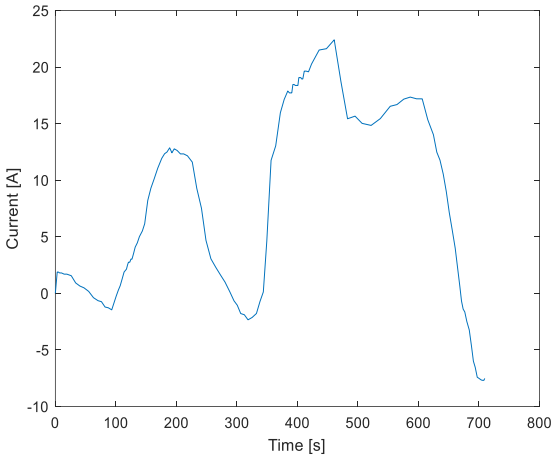

Figure 8 Current profile in the motor with the fixed route. Negative currents correspond to the motor going downhill, therefore, regenerating.

Additionally, leveraging the gathered mechanical data, the electrical power of the scooter has been computed by factoring in the efficiency of the DC-DC converter, as determined in the POWER AND THERMAL LOSSES STUDY section. This involves establishing a connection between the mechanical power of the motor and the electric power of the battery. Since efficiency is subject to variations based on factors such as mechanical torque and angular speed, an efficiency map has been generated. Employing this map, the electrical power depicted in Figure 8 has been derived.

IV. TRACTION SYSTEM

A. *Controller*

It is necessary to develop and implement a controller aimed at regulating the motor's output current. The practical execution of this control involves manipulating the duty cycle of the Pulse Width Modulation (PWM) modulator that feeds the MOSFETs. This adjustment in the duty cycle aims to regulate the voltage supplied to the motor. This control process is based on a set of precise measurements of voltages and currents within the system, serving as key information for the control algorithm.

In this scenario, the controller plays a fundamental role in interpreting the obtained measurements and dynamically adjusting the PWM to keep the motor's output current within the desired limits. The relationship between input and output variables is precisely managed through continuous feedback provided by the system's measurements.

1) *Specifications*

In the specified case, the motor exhibits a dynamic range between -27A and +27A. This range knowledge serves as a foundational parameter for designing a control system that can effectively modulate the motor's operational current within these limits, TABLE II.

TABLE II
CONTROLLER LIMITATIONS

Maximum overshoot, M_p	20 %
Maximum settling time, t_s	13.4 ms
Current max/min	±27 A
Settling time error margin	2 %
Closed loop steady state error	0 %

2) Design

For the design of the system, it must be analyzed the equivalent circuit of the DC motor.

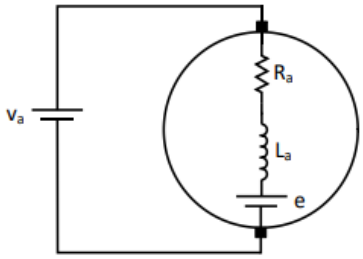

Figure 9 There is an input voltage that enters to the motor. The motor has an internal resistor, inductance and EMF voltage, that is going to be related with the mechanical part, that is, the angular speed multiplied by a constant.

Then, considering the equivalent circuit, the equations that define that circuit are the next ones. One related to the total voltage of the motor (8 and the other related to the electromotive force (EMF) (9.

$$v_a(t) = R_a I_a(t) + L_a \frac{di_a}{dt} + e_a(t) \quad (8)$$

$$e_a(t) = K_e \Omega_m(t) \quad (9)$$

So, in order to obtain the transfer function in the Laplace domain that defines the electrical system that relates the input voltage with the current, the equation needs to be LTI: Linear Time Invariant. Precisely, the model needs to be linear, because to obtain the function it is needed to obtain all the variables, and time invariant. In this case, even if the equations are time invariant, the system is not linear, because the EMF cannot be calculated considering just the electric part of the system. Therefore, we have neglected it, obtaining the following linear equation (10.

$$v_a(t) = R_a I_a(t) + L_a \frac{di_a}{dt} + e_a \quad (10)$$

In addition to the aforementioned considerations, the equation can be isolated into Laplace domain, getting the relation between the output (motor's current) and the input (motor's voltage) of the controller, obtaining the following open loop first order equation (*11*.

$$G(s) = \frac{1}{L_a s + R_a} \quad (11)$$

Furthermore, to analyze the response of the system, the parameters of the DC motor have to be taken into account. For that, some tests have been done that consisted on putting two faced motors: the one that is going to be controlled and the one needed to rotate it. The tests that were done are attached in the next excel file 'PARAMETERS CHARACTERIZATION.xslx' In those tests some measurements have been taken, and then, the parameters shown in the TABLE *III* were obtained .

TABLE III
PARAMETERS OBTAINED FROM THE CHARACTERIZATION TESTS

Motor voltage constant, K_e	0.0749 V/(rad/s)
Armature resistor, R_a	0.137 Ω
Armature inductor, L_a	918 µH
Viscous friction, D	0.0002 Nms/rad
Motor friction coefficient, K_f	0.0997 Nm
Total moment of inertia, J_m	0.00498 kgm²

Moreover, taking into account the parameters of the system, for the reason that it is a first-order system, as it was mentioned before, we can obtain the time characteristics of the electric system, the time constant (τ) and the static gain (k) due to an equivalent equation (12.

$$G(s) = \frac{k}{\tau s + 1} = \frac{\frac{1}{R_a}}{\frac{L_a}{R_a} s + 1} \quad (12)$$

The values of those constants are shown in the TABLE *IV*.

TABLE IV
TIME CHARACTERISTICS

Static gain, k	7.278
Time constant, τ	0.0067 s

The primary requirement for the system is to achieve zero steady-state error, indicating the need for either the plant or the controller to possess a pole at the origin, thereby categorizing the system as a class 1 system. Given that the original plant lacks this characteristic, the chosen controller must incorporate this feature. Consequently, the solution

involves opting for a Proportional Integral (PI) controller for a step response. This type of controller, by virtue of its integral component, introduces the essential pole at the origin, aligning with the requisite for a class 1 system and ensuring the attainment of a zero steady-state error in the overall system response. So, knowing this, the controller equation would be the next one (*13* .

$$C(s) = K_p + \frac{K_i}{s} \quad (13)$$

Having chosen the controller, we have obtained the closed loop ideal transfer function, *(14)*.

$$G_{CL}(s) = \frac{C(s)G(s)}{1 + C(s)G(s)} = \frac{{\omega_n}^2}{s^2 + 2\xi\omega_n s + {\omega_n}^2} \quad (14)$$

In the initial stage of isolating the values for K_p and K_i, it is imperative to derive the values of ξ and ω_n through specific formulas that satisfy the given requirements. These formulas, essential for fulfilling the criteria, are presented below .

$$\xi = \frac{-\ln\left(\frac{M_p}{100}\right)}{\sqrt{\sqrt{ln^2}\left(\frac{M_p}{100}\right) + \pi^2}} \quad (15)$$

$$\omega_n = \frac{4}{\xi t_s} \quad (16)$$

Subsequently, an observation has been made regarding the inadequacy of the initially assigned values for K_p and K_i, as they do not meet the specified requirements due to being non-real values. In response to this, a strategic approach has been taken, involving the utilization of a simulation tool called Sisotool, integrated within the Matlab environment. Within the Sisotool simulation, a meticulous adjustment of the K_p and K_i values have been conducted iteratively until they satisfactorily align with the defined system requirements [7]. Those adjusted values are mentioned in the TABLE V.

TABLE V
CONTROLLER´S KP AND KI CONSTANTS

K_p	1.6918
K_i	952.6526

Hence, presenting the ultimate form of the transfer function for the closed-loop electrical system, incorporating the fine-tuned values of K_p *and* K_i

$$G_{CL}(s) = \frac{0.4297s + 250.6}{0.000918s^2 + 0.5671s + 250.6} \quad (17)$$

(17)

3) Implementation

In the process of implementing the electrical system in the reality, a comprehensive approach was taken to gather essential data. Specifically, the voltage of the battery and the current of the motor were meticulously measured using a combination of a Hall effect sensor and a voltage divider. These measurements, vital for completing the system's loop, were then seamlessly adapted to interface with the TI Delfino F28379D microcontroller.

Within the microcontroller, a sophisticated system of calculations was executed to facilitate the completion of a closed-loop control system. This intricate system relied on the current reference input, regulated by a Proportional-Integral (PI) controller. The role of the PI controller was pivotal in ensuring precise control of the motor's current, aligning it with the desired reference values.

The PWM signals of the MOSFETS were controlled with a voltage source for the measurements of the simulation. The scheme that has been done for completing the system in the microcontroller with the PI controller integrated is shown below.

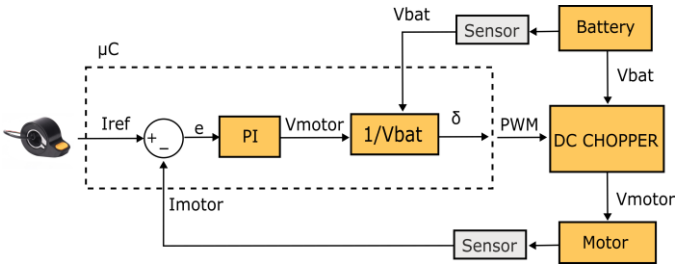

Figure 10 It was needed the current reference as an input and the output should have been the voltage that would enter into the motor, with values between 0V and 24V. Between the current reference and the output voltage there should be the controller, regulating the voltage depending on the current reference and the measured motor's current. And finally, a relation of the output voltage and the measured voltage of the battery should define the duty.

Finally, the simulation was done with the microcontroller, but with protection saturation blocks to limit the current and DUTY CYCLE. For the sample time, it has to be known that the measurements should be received in the ADC blocks of the microcontroller minimally in one period of PWM period time to do the correct response, so 50μs of measurements sample time has been chosen for this case (period corresponding to the switching frequency of the PWM). The comparation of the simulations of the system's response to a step of 5A reference in Matlab and in the reality is shown below.

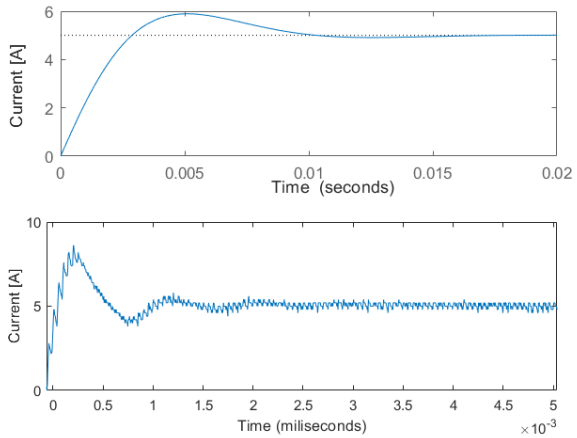

Figure 11 The graph that is seen on the top is the simulation that have been developed in Simulink with the values of the PI controller that are mentioned in the TABLE V, and the one that is seen at the bottom is the graph of the simulation that was done in the reality, with the same values of the PI controller. It was measured by one of the cables of the motor with a current sensor that filled with the oscilloscope. Thus, in accordance with the anticipated expectations and simulated parameters, the graphical representation should ideally exhibit a maximum overshoot of approximately 20% as in the top graph. Additionally, the settling time, a crucial metric for system stability, was expected to be around 13.4 milliseconds. But it is seen that the overshoot of the reality graph is higher than in the specifications, specifically a 35% higher.

4) Validation

As it was seen in the reality graph (bottom graph of the figure x) , the settling time fills with the specification, but, regarding to the overshoot, it reaches 56%. In order to have a lower overshoot, it was decided to reduce the Kp value, specifically 35%, because it is directly related to the overshoot while the Ki is related to the settling time. So the final response that was measured in the reality with the adapted PI controller seemed like in the following (figure y).

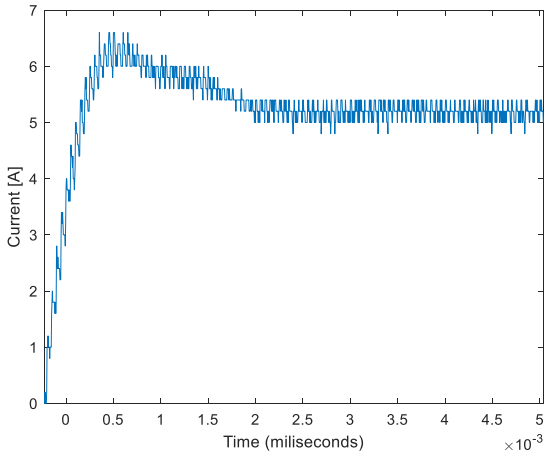

Figure 12 The value of the overshoot was decreased 35%, so the system had a better response regarding the specifications, decreasing the overshoot to 20%. Nevertheless, it established in the limit of the overshoot which is not as it was expected, but if Kp was more decreased the response did not change.

B. POWER DEVICES

Concerning the electronic circuits within the system, a DC Chopper has been employed for supplying power to the motor, as previously mentioned. Additionally, various measurements of current and voltage were conducted, which cover battery voltage, battery current, and motor current (the controlled variable). All these circuits have been integrated into a printed circuit board.

1) Functioning of the DC Chopper

The DC Chopper functions as a DC converter tasked with chopping a DC input voltage to generate an output voltage with a controllable average value. This output voltage is utilized by the motor. In terms of the motor's torque and speed, the system can operate in four distinct states or quadrants [8], Figure 13. In this scenario, the intended application necessitates the motor to function both as a motor and as a generator, enabling the consumption and regeneration of energy. To accommodate this requirement, the application is designed to operate in two quadrants (first and fourth), yielding positive and negative currents, respectively, [9]. To achieve this, the DC-DC converter had to be implemented with two MOSFETs—one at the top and one at the bottom (low side and high side) considering that when one MOSFET is working, the other one is off.

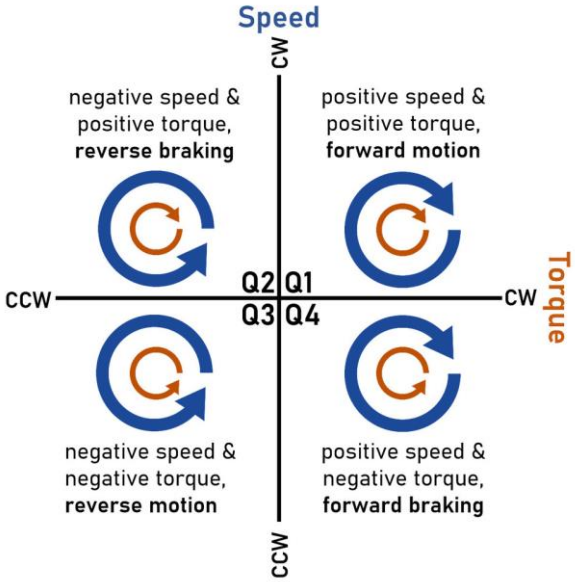

Figure 13 Cuadrants of a DC Chopper. In the application forward motion and forward braking are used.

With the aim of having the DC Chopper working consistently, the components of the PCB were analyzed. For the system to be able to set in motion the motor and to regenerate when necessary.

2) Component specifications

To obtain the desired results some specifications were set. Some of them are imposed from the devices such as

MOSFET, driver…TABLE *VI*, TABLE *VII*. Others are set for a specific purpose, TABLE *VIII*.

TABLE VI
N-CHANNEL MOSFET SPECIFICATIONS

Gate Charge (Q_G)	133 nC
Gate-Source Turn-on Voltage (V_{GGon})	15 V
Threshold Voltage (V_{GSth})	3 V
Plateau Voltage ($V_{GS,pl}$)	4.7 V

TABLE VII
HALF-BRIDGE GATE DRIVER SPECIFICATIONS

Source Bias Current (I_{HBS})	133 µA
Diode Forward Voltage (V_F)	0.85 V
Maximum Gate Current (I_{Gmax})	3 A
Bias current (I_{HB})	0.4 mA

TABLE VIII
CHOSEN SPECIFICATIONS

Switching frequency (f_{sw})	20 kHz
Maximum duty (δ_{max})	% 95
On time (t_{on})	%0.5 T_{sw}
Off time (t_{off})	%0.5 T_{sw}

Additionally, there are two more specifications related to the measurements set by the TEXAS microcontroller and the DC motor. The first one, sets its input to a 0-3 V range. Conversely, the motor sets a range of ±27 A and 0-29 V for its working values.

3) Design

Firstly, starting with the design, it must be known that voltage and current from the battery and the motor must be measured, so, two methods have been employed: the voltage divider for voltage and the Hall-type current sensor. These methods were chosen based on the TABLE and TABLE *X* below, which describes the advantages and disadvantages they entail in relation to the DC chopper system that has been created. The values have been controlled by the microcontroller, so the voltage of each measurement should adapt to between 0V and 3V. To achieve this, protection devices such as amplifiers have been implemented. These amplifiers do not provide gain but ensure that the voltage after adaptation fluctuates between 0V and 3V. Those amplifiers are powered by 0V and 3V with a decoupling capacitor to stabilize that powered voltage. In addition, they were used lowpass filters in the output of those protection amplifiers to attenuate high frequencies, because the interesting signals are the ones that have the lowest frequencies.

TABLE IX
ADVANTAGES AND DISADVANTAGES OF THE VOLTAGE DIVIDER

Advantages	Disadvantages
Simplicity	Load on the measured circuit
Low cost	Sensitivity to changes in resistance
Low power consumption	Influence of temperature
Good accuracy in system's ranges	

TABLE X
ADVANTAGES AND DISADVANTAGES OF THE CURRENT SENSOR

Advantages	Disadvantages
Non-intrusive measurement	Cost
Isolation	Temperature sensitivity
Low consumption	Limited resolution
Wide frequency response	

A voltage divider consists of of measuring reduced voltage by resistors connected in series between the positive side and the reference side of the voltage source. This is useful to work with a microcontroller because the voltage is limited and it cannot enter more than 3V to the microcontroller. So, with that method, the system's battery input voltage and motor's voltage can be reduced to a range of between 0V in the minimum input voltage, and 3V in the maximum input voltage to measure it by the microcontroller. The equation of the relation between the input voltage (V_{in}) and the voltage that is going to be measured (V_{bias}) in a two simple resistors in series (R_2 and R_1) is mentioned below *(18*:

$$V_{\text{bias}} = V_{\text{in}} \frac{R_2}{R_1 + R_2} \quad (18)$$

Regarding to the hall effect current sensor, it has to be said that this sensor measures currents between -30A and +30A detecting magnetic fields and producing an electrical output proportional to the intensity of the magnetic field it is experiencing. So, that sensor automatically converts that range of real current into 0V and 3V being 1.65V 0A and having 33.3mV/A relation.

Secondly, The PCB circuit diagram prompted a thorough examination of its components, with a specific focus on the Driver for correct DC-Chopper operation. The Driver, an electronic circuit managing PWM signals from the

microprocessor for the DC-Chopper, utilized a bootstrap configuration in this application.

When applying a PWM signal to the MOSFET gate, referencing it to the source is crucial. While the low side MOSFET achieves this by connecting to the converter's GND, the high side MOSFET's source, linked to the other semiconductor's drain, lacks a proper reference. To address this, a virtual GND is established through a bootstrap circuit comprising a resistor, diode, and capacitor. This capacitor charges when the low side MOSFET is on and acts as a voltage source, referencing the high side MOSFET's source to the Driver when switched off. This connection effectively creates a virtual GND, Figure 14.

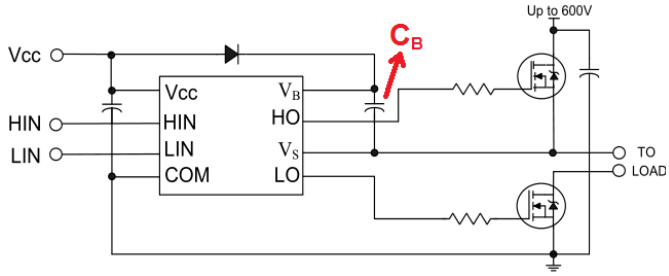

Figure 14 Half-bridge gate driver schematic. Working mode of the Bootstrap.

Consequently, components for the bootstrap configuration were procured through a systematic process, including the acquisition of the capacitor, with equations,*(19),(20)* (*19*) (*20*).

$$Q_T = Q_G + I_{HBS}\left(\frac{\delta_{max}}{f_{sw}}\right) + \left(\frac{I_{HB}}{f_{sw}}\right) \quad (19)$$

$$C_{boot} = \frac{Q_T}{\Delta V_{CB}} = \frac{Q_T}{1.5\ V} \quad (20)$$

As well, concerning the resistor of the bootstrap it shall be known that it was calculated a minimum value with equation. (*21*) However, the value of this resistor is not relevant, as it should be between 0-6 Ω and our calculation resulted into a very small value. It is possible to put 0 Ω into it.

$$R_{boot} = \frac{(1-\delta)T_{sw}}{5C_{boot}} \quad (21)$$

Finally, the design of the gate resistor was done. The final value of it is limited to 10Ω. After the analysis it resulted to be in a range of 5-26Ω. For a deeper analysis with its calculations check '*PCB design'* MATLAB code.

4) Implementation and validation

a) Power losses

After stablishing the circuit parameters, a comprehensive investigation into the power losses of the system has been carried out. The aim of this investigation is to develop an efficiency map and along with this analyze the circuit thermically.

Firstly, along with all the variables from all the tables below a switching frequency was selected in TABLE *VIII*. Its value was limited in order to reduce power losses and considering it the limit audible to the human ear.

In addition, a MATLAB code was created to calculate different cases of efficiency depending on the duty and the battery voltage. Also, as mentioned before, the system is limited to a ±27 A current. The MATLAB code is also working on those limitations. It was also necessary to distinguish between the two stages of the motor. The first one is when it is working as motor (first quadrant) and generator (fourth quadrant), changing its efficiency.

Finally, once all the calculations of the power losses were done (MOSFET, diode…) [10], the efficiency was obtained. Along with this a 3D efficiency map was graphed, Figure 15.

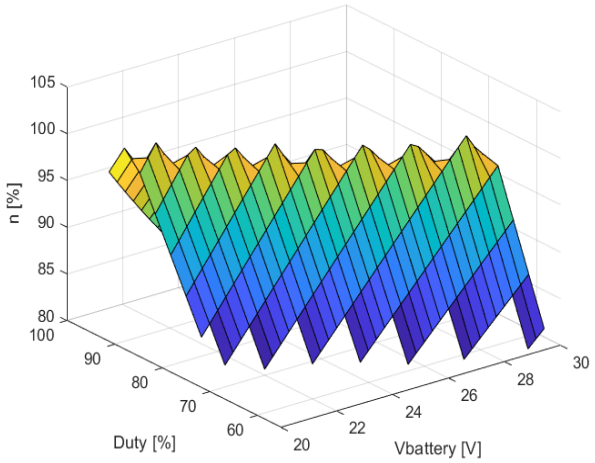

Figure 15 Efficiency map for the system with all its requirements.

Concerning the Figure, it is concluded that the efficiency does not follow a constant structure. In simpler terms, as the battery voltage goes up, the efficiency of the system also goes up. When looking at the Duty Cycle, the system operates most efficiently in the 60% to 90% range. However, it is important to note that if the Duty Cycle is at its highest or lowest values, the efficiency decreases, reaching a minimum efficiency of 85%.

b) Thermal analysis

Because of power losses, a thermal analysis was done in order to discuss the implementation of a heat sink. Therefore, the maximum losses of the system were used for the analysis. The aim of this was to rate the system on its critical point. The maximum value of power losses reaches 5.5 W. The objective was to determine if the MOSFETs could withstand elevated temperatures. With a maximum semiconductor temperature of 175ºC (with a margin of 50ºC), 18 Ω heatsinks were implemented in each MOSFET. In this case, a temperature of 128ºC is obtained, 50ºC far from the maximum. However, the analysis was done in order to analyze a case where there were not heat sinks. In this case, the results explained that a heat sink of 19 Ω was needed, very similar to the one was used.

Additional calculations are detailed in the Thermal Analysis inside *'Power losses'* MATLAB code.

V. ENERGY STORAGE SYSTEM

In context of electromobility, the vital aspect is specifying the energy source. The scooter's power is derived from a electrochemical battery connected to a converter, collecting its characteristics at the TABLE XI.

TABLE XI
BATTERY CHARACTERISTICS

Capacity	12 Ah
Voltage	24 V*
Technology	Li-Ion
Weight	2.4 kg

**Voltage range between 29.4 V (End of charge voltage) and 20 V (End of discharge voltage).*

To improve the model, the elements were considered as variables, being dependent on the State of Charge (SoC) and the C-rate. However, as the values are unknown, three different tests were done: Open Circuit Voltage (OCV) test, parameters test and real profile test.

A. OCV discharge and linear interpolation test

Firstly, the OCV's discharge test was made so the capacity of the battery could be gotten. Even if the battery's original nominal capacity of 12 Ah was stated by the manufacturer, it's likely that the battery had aged, so the OCV's discharge test was used to see if the capacity stays at its initial point.

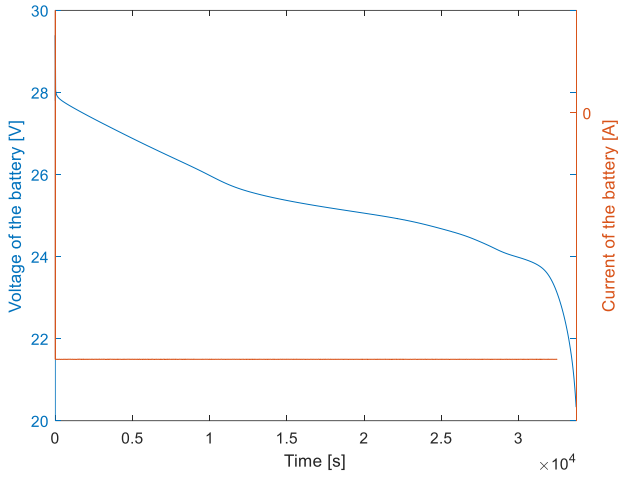

Figure 17: OCV discharge test where the battery was left discharging it whole capacity until reaching the minimum voltage.

Given that discharging at 1/10 C should take 10 hours, the test duration in this case was 33723 seconds, less than ten hours, showing a capacity smaller than 12 Ah. The real capacity was obtained by using equation *(22) (22)* .

$$Q_{\mathrm{n}} = \frac{\sum I(t)\ t}{3600} = 11.243\ Ah \qquad (22)$$

As a result, it was determined that the battery's real capacity was 11.243 Ah. This decrease, as previously shown, this reduction indicates that the battery has degraded.

After that, the OCV was determined based on the SoC through the implementation of the linear interpolation test. This test consists of charging and discharging the battery with a constant current of C/10 to minimize the difference between the OCV and the battery voltage. Given that SoC is an estimated parameter rather than a physical one, the maximum voltage, 29.4 V, is treated as 100% SoC, whereas the minimum voltage, 20 V, is considered as 0%.

This is done considering the internal components of the battery, which include 3 resistors and 2 capacitors, as shown in Figure *18* . The relation of both voltages can be seen in the equation (

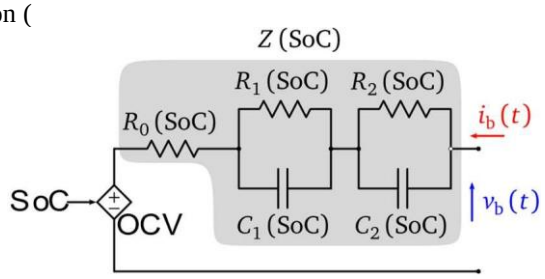

Figure 18 Equivalent electric circuit, with a 2RC model implemented.

$$V_b(t) = OCV(SoC) + R_0 i_b(t) + V_{C1}(t) + V_{C2}(t) \qquad (23)$$

After both tests finished, the average voltage from these tests must be calculated to reduce the effect of hysteresis. It was possible to calculate the OCV with accuracy by using this averaging process.

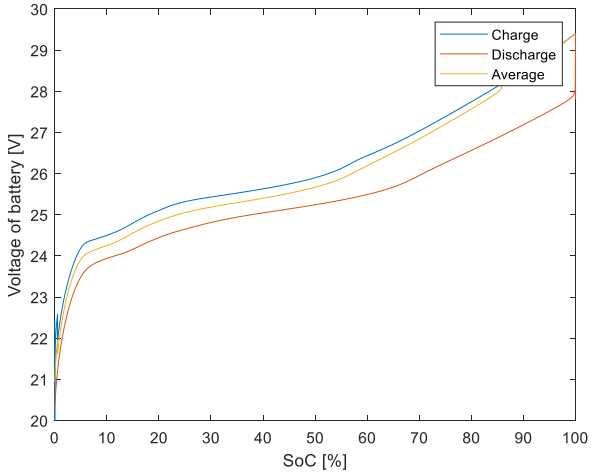

Figure 19 OCV curve showing both discharge and charge test and the hysteresis appearing between them.

B. *Parameter test*

The third test carried out was the parameter test. In this case, a pulsed current of 1C was applied to completely discharge the battery.

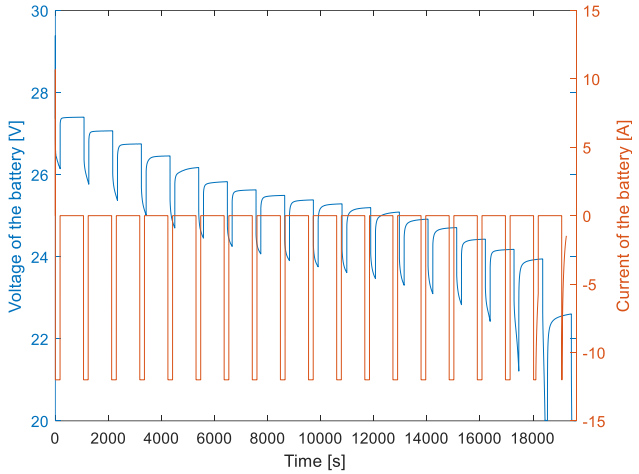

Figure 20: Battery pulsed test relating to 20 pulses of 3 minutes each and a resting state of 900 seconds

The test consists of a cycle of introducing current for three minutes, resting for fifteen minutes, repeating this process until it was fully discharged, as shown in *Figure* 20. As it was thought, the voltage measured during this test shows an exponential pattern. When subjected to negative current, it decreases exponentially and the gradually rebounds to a higher value. Using these current and voltage profiles, an equivalent electrical circuit was created. Thanks to the parameter estimator application, the values of the elements were obtained so that they could be compared to the results of the parameter test. As a result, the model was simulated, obtaining the results of the *Figure* 21.

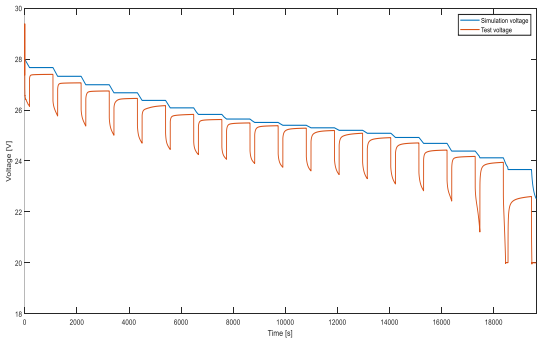

Figure 21: Voltage comparison between the designed model and the real case of the battery.

As we can see in the *Figure* 21, the produced model doesn't match the reference with the accuracy wanted, seeing a little error when comparing the test data with the simulated results. As *Figure* 22 illustrates, the error shows an increase as the SoC decreases.

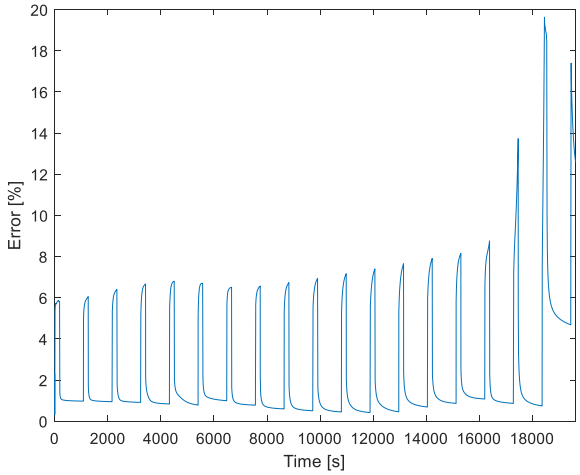

Figure 22: Error comparison between the designed model and the real case of the battery

However, the last test was run to confirm these estimations. It was verified that, when put through the test used for parameter estimation, the model could predict the real voltage with accuracy. This does not, however mean that the model will operate precisely in predicting voltages for every profile. In a final test, an alternative profile was used to evaluate this. The normal daily route's current profile was obtained and used on the battery. The resulting voltage profile was then compared to the one obtained through simulation, verifying the model. This test was also used to evaluate whether it could correspond to the route's requirements. As a result, the forms seen in *Figure* 23 were obtained.

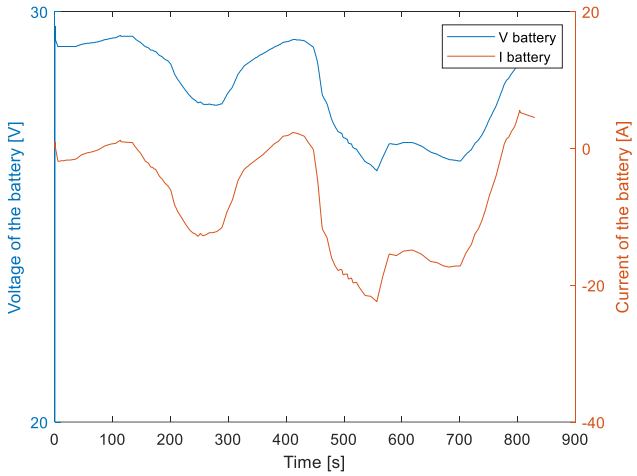

Figure 23: Scooters´ current profile consumption obtained from the chosen route from System energetic analysis chapter.

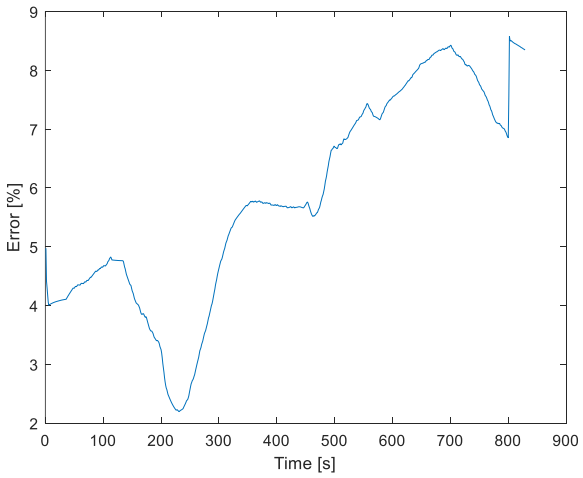

Figure 24: Current profile's error compared t the designed model's response.

It has been verified that actual current profile is achievable. In this case, the SoC of the Figure 25 was obtained.

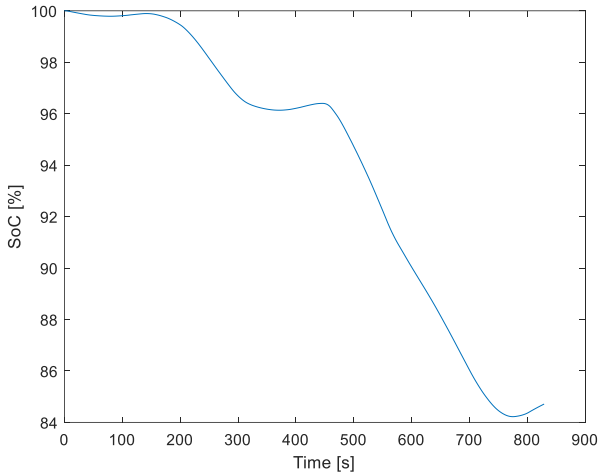

Figure 25: SoC of the daily route profile. The route ends with a SoC of 84.22%.

VI. CHARGING STATION

The scooter we have designed is intended for use by the residents of Donostia, facilitating their commute from the city center to Bidebieta. In Bidebieta, a football field and a gym will be available for people to training. The charging station for these scooters is meticulously crafted to accommodate the simultaneous charging to 20 scooters, and it will be powered by photovoltaic (PV) panels, selected panel are SHARP NA-E125G5 PV.

The charging station's design incorporates sustainability by relying on clean energy sources, with PV panels supplying the necessary power. The careful consideration of environmental impact aligns with the city's commitment to green and eco-friendly initiatives.

To determine the energy requirements for each scooter, an in-depth analysis of the scooter's route was conducted. The data obtained revealed that each scooter will need approximately 16.5 Wh per day to support its daily route.

In order to accurately size the PV panels, extensive data on the irradiance levels in Donostia throughout an entire year has been gathered. This comprehensive dataset will play a crucial role in optimizing the solar power infrastructure, ensuring a reliable and sustainable energy supply for the scooters as they navigate the vibrant streets of Donostia.

The obtained irradiance data for each month is represented in the *Figure* 26.

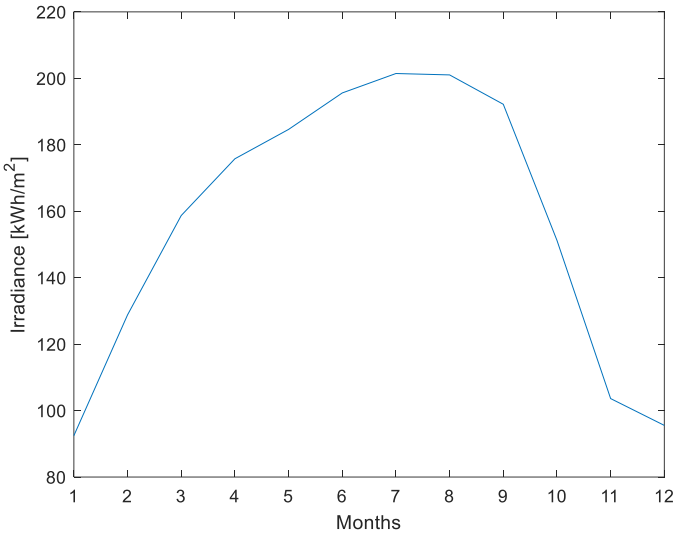

Figure 26 The graph illustrates the monthly solar irradiance levels in Donostia. Given the variation, especially in the summer months, sizing the station considered both yearly and monthly data for optimal design.

Using the provided data, the energy per square meter that the panel can generate was calculated with the equation *(24)* .

$$E_{\text{used}} = Irrad \cdot \eta \qquad (24)$$

The efficiency of these panels is 0.089. Considering each panel has an area of 1.40 m^2, the application required only one PV panel to generate sufficient energy every month. This calculation was performed by determining the monthly energy requirements for the scooters and then estimating the corresponding area of PV panels needed to meet these energy needs.

Given that energy generation occurs during the day while scooter charging takes place at night, stationary batteries were integrated into the charging station. These batteries store the energy generated during the day to facilitate scooter charging overnight. The chosen battery for storage is the Lithium LiFePO4 24V 100Ah battery.

To determine how many batteries would be needed for our charging station to accommodate 20 scooters, we first established the estimated charging time for the scooters, set at 5 hours to avoid potential degradation of the scooter batteries due to faster charging.

With this information, we calculated the power needed for the scooters, which is the total energy required by all scooters over a 5-hour period. We oversized this power calculation by 50% to allow for more flexibility in future adjustments, such

as accommodating additional scooters or reducing the charging time.

$$P_{\text{scooter}} = \frac{E_{\text{scooters}}}{T_{\text{charge}}} 1.5 = \frac{330}{5} 1.5 = 99W \quad (25)$$

We then performed a similar calculation for the lithium battery that will be installed, determining its power by the following equations,(26)(27).

$$P_{battery} = V_{\text{battery}}\, I_{\text{battery discharge}} \quad (26)$$

$$P_{battery} = 25.6 \cdot 50 = 470W \quad (27)$$

By comparing the powers of both batteries, we can ascertain how many batteries would be required in our charging station. In this case, it was determined that a single battery is sufficient to meet the charging needs of all 20 scooters.

After determining the appropriate size for the PV panels and batteries, an evaluation of the overall installation cost for the charging station has been conducted. This process involved meticulous consideration of the materials and applications essential for enhancing the efficiency and functionality of the entire system.

Initiating the setup, a DC/DC converter would be seamlessly integrated directly into the PV panels. This strategic placement ensures optimal energy conversion from the solar panels. Subsequently, charge controllers would be deployed to govern and regulate the charging process between the PV panels and the battery, ensuring a smooth and efficient transfer of energy.

Continuing the sequence, an additional DC/AC converter would be employed. This component serves a dual purpose, facilitating the charging of the electric scooter while also allowing surplus energy to be seamlessly fed back into the grid. This surplus energy is intended to be sold, contributing to the overall sustainability of the charging station.

In terms of protection, a multi-layered approach has been adopted. Fuses play a crucial role in safeguarding the system by preventing overcurrent situations, thus preserving the integrity of the components. Overvoltage protection mechanisms are also implemented to shield the installation from voltage spikes, ensuring the longevity of the equipment.
Completing the installation, meticulous attention is given to the wiring and switches, ensuring a well-organized and efficient electrical setup.

The structural integrity of the entire system, encompassing both the PV panels and the charging station, is upheld by sturdy supports designed to withstand environmental conditions. In the TABLE XII, the components we will be using, and their respective prices are displayed:

TABLE XII
instalation cost

Element	Cost
SHARP NA-E125G5 PV PANEL	55€
Lithium LiFePO4 24V 100Ah	469.99€
MPPT SOLAR CHARGE CONTROLLER 40/50/60 / 100A, 12V 24V PANNEL BATTERY CONTROLLER REGULATOR	31€
INVERSOR VICTRON PHOENIX 24V 3000VA SMART	818.53€
ICTRON BLUESOLAR MPPT REGULATOR 75/15	47.99€
Midi-fuse Victron 150A/32V	10.66€
SOLAR COMBINER BOX, WATERPROOF ISOLATOR SWITCH	50.15€
10AWG Solar Panel Cable	12.99€
Connector Kit	
Support	71.17€

The total cost of the installation amounts to 1567.5€, but with a 50% government subsidy, it reduces to 783.74€. As previously mentioned, the PV panels operate during daylight hours, occasionally generating excess energy. This surplus is fed back to the grid, earning us a reimbursement of 0.17€/kWh. However, the reimbursement is limited to 150% of our consumption, totaling 14.85KWh per month, equivalent to 2.525€.

To better assess the financial implications, we must consider not only the earnings from contributing energy to the grid but also the savings achieved by using our self-generated energy instead of relying on the grid, priced at 0.25€/kWh. In total, our monthly savings reach 5€.

In conclusion, the amortization period for the entire charging station system will be 13 years and one month, factoring in both earnings and savings.

To better assess the financial implications, it's essential to note that if our consumption were to increase, perhaps by adding more scooters or utilizing the charging station for other applications, the 150% compensation from returning surplus energy to the grid could result in greater financial returns. This could potentially expedite the amortization period of the entire system, making it a more lucrative and efficient investment.

VII. AIR CONDITIONING SYSTEM

As previously highlighted, our upcoming charging station will serve as the hub for recharging the scooters' batteries. Preserving the longevity and performance of these batteries is paramount, necessitating the maintenance of an optimal temperature and humidity within the charging environment to mitigate degradation. To address this, we have meticulously crafted and implemented an advanced air conditioning system.

This system is engineered to intelligently assess the internal conditions of our charging station continually. It dynamically adapts, manipulating the properties of the external air it draws

in to align precisely with our predefined environmental objectives. By doing so, the air conditioning system acts as a safeguard, creating an atmosphere conducive to minimizing battery degradation and optimizing their overall health. This proactive approach ensures that our charging station not only facilitates efficient scooter charging but also prioritizes the sustained well-being of the batteries in the process.

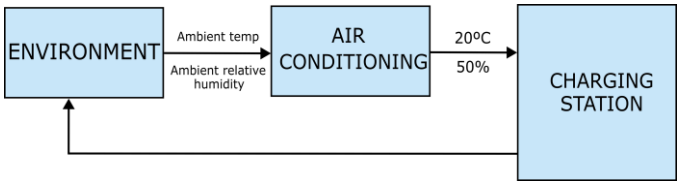

Figure 27 Block diagram of the charging station air conditioning circuit. We take air from the environment, adapt it to our desired conditions by cooling or heating it, and finally introduce it to the charging station plant.

A. *Specifications*

The optimal climate for storing batteries that undergo constant cycling, particularly those based on lithium-ion technologies, is identified as a temperature of 20ºC and a relative humidity level below 50%. Maintaining these specific environmental conditions is crucial for preserving the performance, longevity, and safety of the batteries. This ensures that the batteries can consistently operate at their best, minimizing the risk of degradation and maximizing their overall efficiency.

B. *Wheather conditions*

To assess the necessity of implementing a conditioning system, a comprehensive climate study has been conducted specific to the location, which is Donostia. This study aims to understand the local climatic conditions and tailor the choice of a conditioning system to effectively address the unique environmental factors in that area.

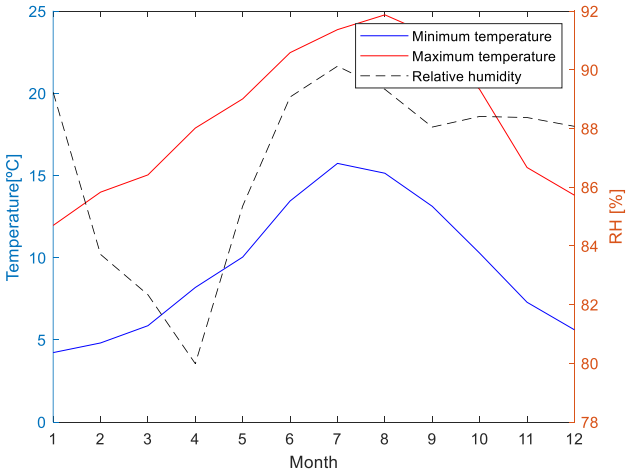

Figure 28 Values of average maximum and minimum temperatures and relative humidity in Donostia from 2014 to 2021.

The analysis leads to the conclusion that heating, cooling, and dehumidification processes are deemed necessary. Additionally, to safeguard operational efficiency, a thorough examination of the identified critical conditions will be conducted collectively.

C. *Air conditioning*

The thermal model of the system is based on the energy and mass conservation principles. Combining them and according to the definition of the specific humidity, we obtain the next equation.

$$\frac{dT}{dt} = \frac{\dot{m}h(T_{in}\omega_{in}) - \dot{m}h(T_{room}\omega_{in}) + \dot{Q}}{M_a(c_a + \omega c_v)} \tag{28}$$

The air conditioning is thought to be an isobaric heating/cooling process at 101.3 kPa. The variable mass is obtained from equation , and it is related with the equation of the mass losses.

$$M_{air}(T) = \frac{V \cdot \mathrm{P_t}}{T \cdot (R_\mathrm{a} + R_\mathrm{v} \cdot \omega)} \tag{29}$$

$$\dot{m}_{\mathrm{loss}} = \frac{-dM_{\mathrm{air}}}{dt} \tag{30}$$

Having to take the air from the environment, we have analyzed the two critical cases we have suffered between 2014 and 2021. Those cases consist on a maximum temperature of 39,1 degrees, a minimum temperature of -5,3 degrees and a maximum relative humidity of 98,5%.

In our case, sizing our system to those critical cases, we will be able to adapt any condition we have. We reach to the conclusion that we need a maximum cooling power of 1877W and a maximum heating power of 1856W.

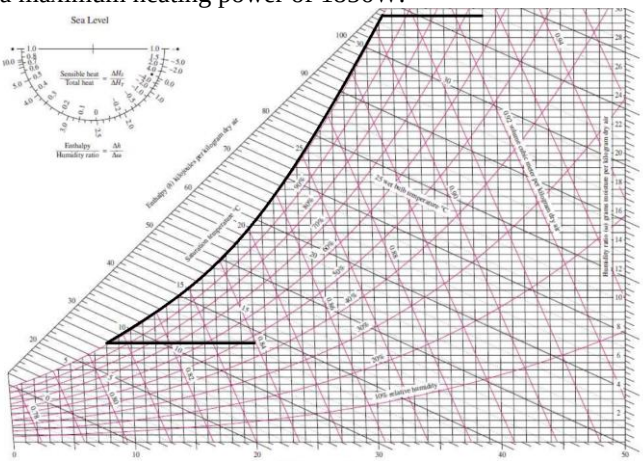

Figure 29 Psychrometric chart of summer critical condition. To lower both the temperature and humidity, our process begins by cooling the air to 8ºC. At this stage, we extract 64g of water per kilogram of introduced air through condensation. Subsequently, we raise the temperature of the air to 20ºC. This not only brings it back to our initial specification but also decreases its current relative humidity from 100% to 50%.

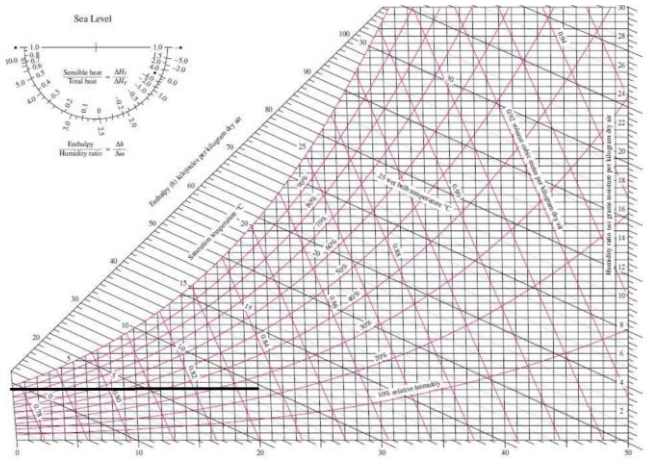

Figure 30 *Psychrometric chart of winter critical condition. To address the low temperature, we need to elevate it to our target of 20ºC. Fortunately, humidity is not a concern at this point. Referring to the earlier illustration, Figure 29 Psychrometric chart of summer critical condition. To lower both the temperature and humidity, our process begins by cooling the air to 8ºC. At this stage, we extract 64g of water per kilogram of introduced air through condensation. Subsequently, we raise the temperature of the air to 20ºC. This not only brings it back to our initial specification but also decreases its current relative humidity from 100% to 50%. it is evident that the maximum temperature attainable with 100% relative humidity is 8ºC. Since our current temperature is below this threshold, the relative humidity will consequently be lower as well.*

Given the absence of internal water sources, it is imperative to maintain a consistent indoor specific humidity, allowing for minor fluctuations resulting from new humidity inputs before returning to stability. Nevertheless, variations in relative humidity are inevitable, primarily attributed to changes in indoor temperature caused by external heat inputs.

Implementing thermal and humidity controls is crucial to guarantee that both critical parameters remain within the predefined ranges once the transient state concludes. To achieve this, it is essential to treat both critical magnitudes independently, ensuring the continuous operation of the air conditioning system even if one of the parameters falls within the established hysteresis range. This approach helps maintain optimal conditions and ensures the stability of the environment.

The speed of the controls' response is contingent on the input volumetric flow rate set for the system. In compliance with the EN 15242 normative and the CTE (Código Técnico de la Edificación), a minimum ventilation requirement of 0.7 L/s m² is mandated by law, especially in the absence of natural ventilation. This legal standard ensures a baseline ventilation level for maintaining indoor air quality and conforms to established building regulations.

We have performed a simulation in which both humidity and temperature are inside the charging station are regulated to our specifications. As previously mentioned, changing the air mass flow rate can determine the time of this transient period until it stabilizes.

VIII. Conclusion

Despite our route being 3.2 kilometers, we have verified that our battery has the capacity to cover a much longer distance. We can confidently say that our objective has been achieved, as the autonomy of our scooter exceeds 4 kilometers.

We have designed a charging station for 20 scooters, and through oversizing, we have increased its capacity to charge even more scooters. Additionally, as mentioned previously, it would be advantageous for us to charge more scooters or even utilize the charging station to meet other energy needs. This way, we could potentially gain greater economic benefits, especially considering government assistance conditions.

We have successfully designed an air conditioning system to adjust the temperature to 20 degrees Celsius and the relative humidity to 50%, as these are the optimal conditions to prevent battery degradation.

Despite aiming for a 97% efficiency in the DC/DC converter, we have only achieved an 86% efficiency due to power losses. Considering our components, this has been our best result obtained.

IX. Future lines

The future lines that can be implemented on the scooter have been analyzed:

A. Greater Battery Autonomy

To enhance the overall user experience and address the growing demand for extended travel capabilities, our research and development team is actively engaged in advancing battery technology. The primary focus is on the creation of higher-capacity batteries that will significantly extend the range of our electric scooters. This improvement not only contributes to customer satisfaction but also aligns with our commitment to sustainable and eco-friendly transportation solutions.

B. Fast Charging Technology

Recognizing the importance of convenience in the daily lives of our users, we are exploring the integration of cutting-edge fast-charging technology. By implementing this feature, we aim to substantially reduce the time required for recharging the scooter's battery. This innovation not only caters to the increasing demand for efficient electric vehicles but also positions our products as a hassle-free and time-saving mode of transportation.

C. Connectivity

Embracing the era of smart mobility, our upcoming product lines are set to feature comprehensive connectivity options. This includes the integration of advanced GPS systems, enabling users to navigate seamlessly through urban environments. Furthermore, Bluetooth connectivity will facilitate easy synchronization with mobile devices, allowing users to manage various aspects of their electric scooters through dedicated mobile applications. Real-time monitoring, performance analytics, and firmware updates can be effortlessly accessed, providing users with a heightened level of control and customization.

D. Sustainable Materials

To promote environmental sustainability and reduce our carbon footprint, we are committed to incorporating sustainable and recyclable materials in the manufacturing process of our electric scooters. By carefully selecting materials that align with eco-friendly principles, we aim to contribute to the global movement towards greener transportation solutions. This not only enhances the appeal of our products to environmentally conscious consumers but also reflects our dedication to responsible business practices.

E. Hydrogen combustion

Hydrogen energy utilizes hydrogen or hydrogen-containing components to efficiently generate energy for various practical purposes, offering significant social, environmental, and economic advantages. To harness this energy, storage systems and devices like fuel cells are essential.

As mentioned, implementing this type of energy source as the primary power supply in the future is a compelling idea, particularly due to its environmentally friendly nature. Additional information about this topic can be found in a separate document.

F. OF-OFF Control for air conditioning

Implementing an on-off control for the air conditioning system to avoid keeping it constantly running. Define a temperature range between 20-25 degrees Celsius and a relative humidity range between 40%-50%, maintaining conditions within these values. This approach not only ensures comfort but also helps reduce electrical energy consumption.

REFERENCES

[1] «Ley 7/2021, de 20 de mayo, de cambio climático y transición energética,» Boletín oficial del estado, 2021.

[2] «race,» 30 Mayo 2005. [En línea]. Available: https://www.race.es/emisiones-co2-coche-que-dice-ley#:~:text=En%202019%2C%20justo%20antes%20de,26%2C9%20%25%20del%20total..

[3] «eSmartcity,» 1 Junio 2016. [En línea]. Available: https://www.esmartcity.es/2016/06/01/el-86-por-ciento-co2-emitido-movilidad-proviene-ciudades.

[4] R. Aguilar, «xataka,» 3 Enero 2024. [En línea]. Available: https://www.xataka.com/movilidad/espana-sigue-prefiriendo-coche-barato-no-electrico-datos-matriculaciones-dejan-sabor-agridulce-para-industria.

[5] «corresponsables,» 29 Septiembre 2023. [En línea]. Available: https://www.corresponsables.com/actualidad/sanitas-120-toneladas-co2-politica-movilidad-sostenible.

[6] «DGT,» 16 Febrero 2023. [En línea]. Available: https://www.dgt.es/muevete-con-seguridad/viaja-seguro/en-patinete/. [Último acceso: 22 Enero 2024].

[7] A. K. G. T. Tako Nama, «Low Power Electric Two-Wheelers for Hilly Region».

[8] «EEEguide,» [En línea]. Available: https://www.eeeguide.com/four-quadrant-operation-of-motor-drive/.

[9] C. Cavallo, 15 Noviembre 2020. [En línea]. Available: https://www.thomasnet.com/articles/instruments-controls/dc-motor-controllers/. [Último acceso: 25 Enero 2024].

[10] M. Mazuela, «POWER LOSSES CALCULATION USING DATASHEET,» 2021.

[11] P. M. S. K. A. S. P. R. S. S. Gaurav Changdeo Andhale, «Design and Development of Electric scooter,» Ahmednagar, Maharashtra, 2020.